

Study on some linear and nonlinear optical parameters of glycine hydrofluoride single crystals

A. ABU EL-FADL*, A.M. ABDEL-SALAM, A.M. NASHAAT

Faculty of Science, Department of Physics, Assiut University, Assiut 71516, Egypt

Single crystal of glycine hydrofluoride (GHF) was grown from aqueous solution by slow evaporation technique. The structure of the grown crystal was tested and analyzed through X-ray powder diffraction. The functional groups have been identified from the FT-IR spectra. Slabs cut normal to the b-axis from the grown crystal were subjected to incident radiation with a wavelength range of 200 nm to 800 nm to investigate the transmittance and reflectance spectra. Linear optical parameters such as extinction coefficient k , refractive index n and both the real and imaginary parts: ϵ_{real} and ϵ_{im} of the dielectric permittivity were calculated as functions of the incident photon energy. The dispersion of the refractive index was fitted in terms of Cauchy formula and Wemple-DiDomenico single oscillator model. GHF crystals exhibited indirect optical interband transition and the optical energy gap E_g was determined by using Tauc plot. The indirect band gaps at elevated temperatures were determined and their temperature dependence was estimated. Optical band gap E_g values were found to decrease with an increase in crystal temperature; however, the band tail width exhibited opposite behavior. The nonlinear optical potential was examined by the second harmonic generation (SHG) test.

Keywords: GHF single crystal; optical energy gap; optical constants; temperature dependence; SHG efficiency

1. Introduction

Amino acid glycine $\text{CH}_2\text{NH}_2\text{COOH}$ salts and crystals draw the attention of crystal growth researchers and experts. As glycine does not exhibit an asymmetric carbon atom, it becomes optically inactive. Glycine based crystals of high optical quality with wide optical band gap values and high dielectric constant are easy to grow from aqueous solutions [1].

Glycine hydrogen fluoride abbreviated as GHF single crystal with molecular formula $\text{C}_2\text{H}_5\text{NO}_2\text{HF}$ was crystallized by solution growth method and the structure of the grown crystal was investigated by X-ray powder diffraction. The obtained lattice constants agree with the earlier reported data for GHF crystal being a member of orthorhombic crystal system with the lattice constants $a = 15.601 \text{ \AA}$, $b = 14.001 \text{ \AA}$, $c = 15.662 \text{ \AA}$ [1].

A study of linear optical parameters at different scales is necessary for providing deep understanding of interaction processes between

the optical excitation and transitions (i.e. electronic excitations) and photon energy [2]. The determination of optical constants is expected to expand the available physical knowledge necessary to fairly characterize materials that are used in the fabrication of optoelectronic devices [3]. The good optical transmittance in the visible and IR regions makes GHF crystal a potential material for optoelectronics applications [4]. In addition, some linear and nonlinear optical parameters of GHF crystal were investigated [5].

The process of monitoring the properties of GHF crystals revealed some particular features of this material. The presence of allowed indirect optical transition, which is common for the crystals grown by slow evaporation technique, was investigated. The studies of optical absorption spectra and optical parameters of GHF crystal were carried out. In addition, optical energy gap dependence on crystal temperature was considered. Non-dispersive refractive index was calculated, while the dispersion of the refractive index in terms of Wemple-DiDomenico single-effective-oscillator and Cauchy models were investigated

*E-mail: abulfadla@yahoo.com

along with other linear optical parameters. The second harmonic generation efficiency of the GHF crystal was calculated to assign the crystal for proper applications.

2. Experimental

2.1. Crystal growing

To start the growing process of GHF, one mole of $\text{NH}_2\text{CH}_2\text{COOH}$ – amino acid glycine – (75.07 g) was dissolved in 250 mL of deionized water and then equimolar ratio of HF (20.2 mL) was added to form a homogenous solution and, when the solution was let to cool, GHF precursor was developed in the crystallizing jar. The precursor from the first step was dried and then dissolved to form a second step solution; the obtained solution was filtered, purified then it was allowed to cool and evaporate at ambient temperature. Nucleation occurred and small crystals were grown at the bottom of the crystallizing jar. Good quality small transparent crystals were grown by successive recrystallization and then collected to employ them as seed crystals. Saturated solutions were taken into a constant temperature crystal growth apparatus and were allowed to equilibrate at 45 °C. Seed crystals were then suspended firmly inside the solution using a nylon thread. The jars containing the solutions were covered in a manner which allowed the solutions to evaporate slowly. After seven weeks, seeds were grown to nearly perfect single crystals, and the crystals having appropriate large size, obtained in this way were pure, and stable under normal conditions of temperature and humidity. The grown crystals were single phase GHF crystals with chemical composition $\text{C}_2\text{H}_5\text{NO}_2\text{HF}$ as confirmed later by further analysis. The final grown crystal was large with about 1.6 cm \times 1.2 cm \times 4 cm in size.

2.2. Structural analysis

Powder X-ray diffraction data were collected for the grown crystals using Philips X-ray diffractometer model PW 1710 with $\text{CuK}\alpha$ radiation ($\lambda = 1.5405 \text{ \AA}$). The operating voltage and current were set to 40 kV and 30 mA, respectively. The scanning rate was maintained at 1° per minute.

2.3. Fourier transform infrared (FT-IR) investigation

NICOLET FT-IR 6700 spectrometer was employed to record the Fourier transform infrared (FT-IR) spectra of the GHF crystal in the wavenumber range of 400 cm^{-1} to 4000 cm^{-1} . The powder samples were investigated by the KBr pellet method.

2.4. UV-Vis spectra

The optical transmittance measurements were carried out using Shimadzu UV-Vis-2101 PC dual beam scanning spectrophotometer in the wavelength range of 200 nm to 800 nm. Samples of a size 0.5 cm \times 0.5 cm \times 0.1 cm were cut with two faces perpendicular to b-direction and put inside a special holder keeping air as reference. A special reflectance attachment, where the sample placed horizontally on the stage facing down was used. It was illuminated from the bottom to perform reflectance measurement. The temperature of the sample was maintained with an accuracy of 0.1 °C using an ultra-thermostat (Mgw Lauda type K2R, Germany).

2.5. SHG efficiency

SHG efficiency was measured using a Q-switched Nd:YAG Laser (Spectra-Physics) with a fundamental wavelength of 1064 nm, input pulse energy of 1.1 mJ per pulse and repetition rate of 10 Hz with a pulse width of 10 ns. The arrangement was provided by means of photomultiplier tube system to collect the output pulse.

3. Results and discussion

3.1. XRD characterization

Fig. 1 shows the indexed X-ray powder diffraction pattern of GHF crystal which makes a good match with the CCDC file number 779604. The diffraction pattern confirms good crystallinity of the obtained crystal as the diffraction peaks are sharp with small bandwidth ranging from 0.13° to 0.58°. The pattern also reveals that the most favorable growth direction is (4 3 0) which is observed and indexed to the diffraction peak around 30°.

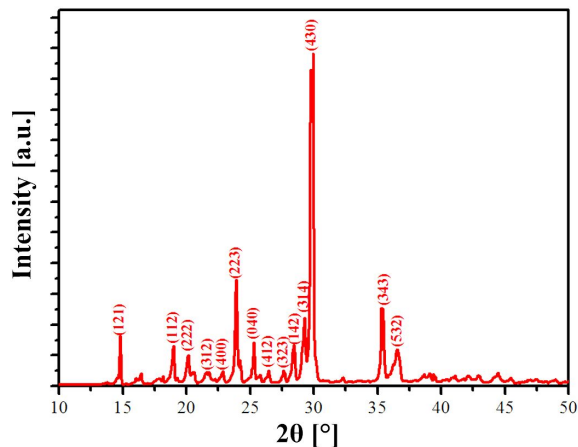


Fig. 1. X-ray diffraction pattern of GHF single crystal.

The lattice parameters and unit cell constants were calculated accurately by a conventional method using the obtained X-ray diffraction data. The refinement employed for the obtained X-ray powder diffraction data and the indexing of the diffraction peaks were matching to *Pbca* space group. The crystal structure after refinement was orthorhombic class system with cell parameters of $a = 15.528 \text{ \AA}$, $b = 14.094 \text{ \AA}$ and $c = 15.749 \text{ \AA}$. The resultant lattice parameters are in a good agreement with the results of Fleck et al. [6] who claimed that GHF crystal belongs to the centrosymmetric space group *Pbca* and should not exhibit second harmonic generation at room temperature. Similar crystal, with a big deviation from another values of lattice constants reported by Vijayan et al. [4] and Selvaraju et al. [5] exhibited second harmonic generation (SHG) with an efficiency higher than that of potassium dihydrogen phosphate (KDP) single crystal.

3.2. FT-IR spectra

The measured FT-IR spectrum of GHF single crystal presented in Fig. 2, demonstrates spectral differences between GHF single crystal and pure amino acid glycine. The figure clearly shows that there are apparent shifts in all peak positions in addition to the change in the shape and intensity of many peaks in the spectrum of GHF crystal compared with pure glycine sample spectrum measured in the same conditions.

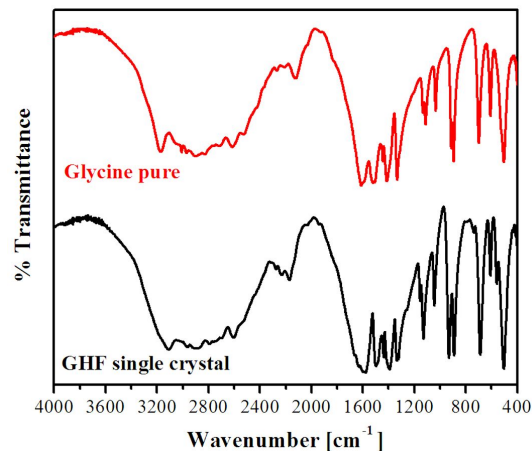


Fig. 2. FT-IR spectra of pure glycine and GHF single crystal.

The assignment of compounds containing carboxyl groups is an extremely difficult process. Different vibrational bands overlap, resulting in the formation of new sharp bands at unexpected positions or broad humps which overcome many bands in the spectra [7, 8]. GHF and glycine samples show a similar spectral trend which exhibits a medium intensity hump spanning from 3400 cm^{-1} to 2400 cm^{-1} typical of many amino acids and this hump can be assigned to amine NH_2 stretching modes (symmetric and asymmetric) with overlapping CH_2 stretching bands. An interesting band is observed at 2123 cm^{-1} for glycine and at 2170 cm^{-1} for GHF which can be assigned to a combination of different vibration modes as pointed out in Table 1.

NH_2 symmetric scissoring and NH_2 asymmetric scissoring bands are located at the doublet 1506 cm^{-1} , 1520 cm^{-1} and 1613 cm^{-1} , respectively, for glycine sample, while the two bands combine to form an intermediate band at 1497 cm^{-1} with extinguishing of the doublet and 1577 cm^{-1} band in the spectrum of GHF sample.

The CH_2 scissoring, wagging and rocking bands are located at 1443 cm^{-1} , 1332 cm^{-1} and 910 cm^{-1} for glycine and at 1437 cm^{-1} , 1335 cm^{-1} and 929 cm^{-1} for GHF, while the bands observed at 698 cm^{-1} , 607 cm^{-1} for glycine and at 686 cm^{-1} , 607 cm^{-1} for GHF could easily be assigned to COO scissoring and wagging

Table 1. Assignment of the FT-IR absorption bands for glycine and GHF single crystal.

Wavenumber [cm^{-1}]		Assignment
Pure glycine	GHF single crystal	
502	502	COO scissoring
	557	H-F in-plane bending
607	607	COO wagging
698	686	COO scissoring
892	889	C-C stretching
910	929	CH ₂ rocking
1033	1043	C-N stretching
1111		NH ₂ rocking
1131	1127	NH ₂ rocking
	1154	C-F stretching
1332	1335	CH ₂ wagging
1412	1391	COO symmetric stretching
1443	1437	CH ₂ scissoring
(doublet) 1506 1520	1497	NH ₂ symmetric scissoring
(doublet) 1506 1520	1577	NH ₂ symmetric scissoring
1613	1577	NH ₂ asymmetric scissoring
2123	2170	combination bands (COO symmetric stretching + COO scissoring)
2895	2890	CH ₂ symmetric stretching
3008	2964	CH ₂ asymmetric stretching
3170	3110	NH ₂ asymmetric stretching

vibrations. The COO symmetric stretching vibration is assigned to the band at 1412 cm^{-1} for glycine sample and this band is shifted to 1391 cm^{-1} in the GHF spectrum. NH₂ rocking vibration can be assigned to the bands at 1111 cm^{-1} and 1131 cm^{-1} for glycine and for GHF single crystal; it is assigned to the band centered at 1127 cm^{-1} .

The bands at 1033 cm^{-1} and 1043 cm^{-1} are assigned to C-N stretching vibration for glycine and GHF, respectively. The bands at 892 cm^{-1} , 889 cm^{-1} are assigned to the C-C stretching vibration for glycine and GHF, while the CCO scissoring vibration bands are found to coincide at 502 cm^{-1} in the two samples.

Monofluorinated compounds show a strong band between 1000 cm^{-1} and 1110 cm^{-1} , and with more than one fluorine atoms, the band splits into two bands, for symmetric

and asymmetric modes [9]. The carbon-fluorine bands are so strong that may hinder the presence of any carbon-hydrogen bands [10]. They may be assigned to the new band observed at 1154 cm^{-1} in the spectrum of GHF.

3.3. Transmittance T and reflectance R measurements

The measurements of transmittance T and reflectance R were performed at room temperature on rectangular thin plates cut normal to the b-axis direction from the grown GHF crystal, in the wavelength range of 200 nm to 800 nm of incident radiation as shown in Fig. 3. It is observed that, transmittance increases gradually with increasing the values of the incident wavelength. The spectrum shows a transmittance cut off value at 232 nm after which the transmittance vanishes, indicating the edge of the band gap. The incident wavelength is absorbed by the crystal in such case.

The total absorption coefficient α can be calculated from the transmittance data using Lambert formulas [11]:

$$I = I_o e^{-\alpha d} \quad (1)$$

$$\alpha = \frac{2.303}{d} \log \left(\frac{I_o}{I} \right) = \frac{2.303}{d} \log \left(\frac{1}{T} \right) \quad (2)$$

where d is the crystal thickness, T is the transmittance and α is the absorption coefficient.

The reflectance spectrum demonstrated in Fig. 3, shows a different trend than that of the transmittance. The reflectance decreases rapidly at lower wavelengths up to 400 nm, and then exhibits a small minimum around 600 nm before it stabilizes at a constant reflectance value around 1.2 % up to 800 nm.

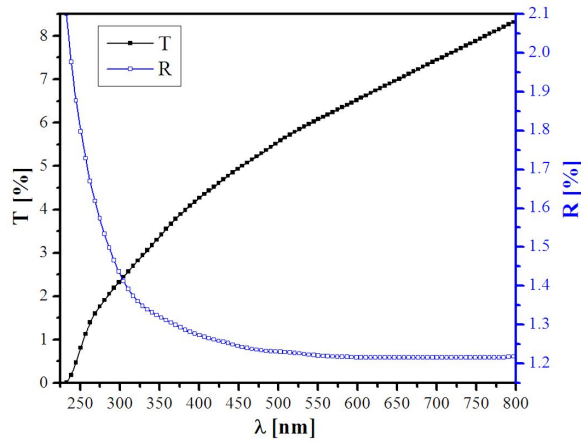


Fig. 3. Room temperature transmittance T and reflectance R spectra for GHF single crystal.

The main observation from the T and R data for GHF crystal is the transparency in the visible and near IR region. The T and R curves intersect at 309 nm in spite of their great difference in values but that intersection point demonstrates the inversion of the interaction mechanism between the crystal and incident radiation from high transmittance to high reflectance and vice versa.

3.4. Linear optical parameters

3.4.1. Extinction coefficient and refractive index

Optical profile of materials can be estimated from optical constants calculation and analysis.

Optical constants are the parameters calculated mainly from transmittance and reflectance data which are considered as linear parameters and their behavior could be predicted to provide information about the interaction of light with the material.

Propagation of electromagnetic radiation in absorbing materials can be described using a dimensionless complex-valued refractive index $n = n + ik$. The imaginary part controls light attenuation within the material and is known as extinction coefficient k . The real part represents refraction or change in the phase velocity of incident radiation and is known as refractive index n .

The refractive index n can be determined by measuring the reflectance from the surface of the material, and could be obtained using relation [12]:

$$n = \frac{(1 + \sqrt{R})}{(1 - \sqrt{R})} \quad (3)$$

The extinction coefficient k determines how fast the amplitude of a wave decays in the material; it is directly related to its absorption and could be calculated from the following equation:

$$k = \alpha \lambda / 4\pi \quad (4)$$

where α is the absorption coefficient and λ is the wavelength of incident light.

Values of k and n are depicted in Fig. 4. It can be noted from the figure that the refractive index n increases with increasing photon energy. The figure also implies that, the extinction coefficient k decreases with increasing photon energy up to 4.346 eV and then continuously increases with increasing photon energy.

3.4.2. Dispersion of refractive index

The values of refractive index n can be fitted reasonably in the strong absorption region ($\lambda \leq 600$ nm) to a three-term Cauchy dispersion relationship [13]:

$$n(\lambda) = A + \frac{B}{\lambda^2} + \frac{C}{\lambda^4} \quad (5)$$

where A , B and C are fitting parameters. Cauchy dispersion works best for crystals and materials

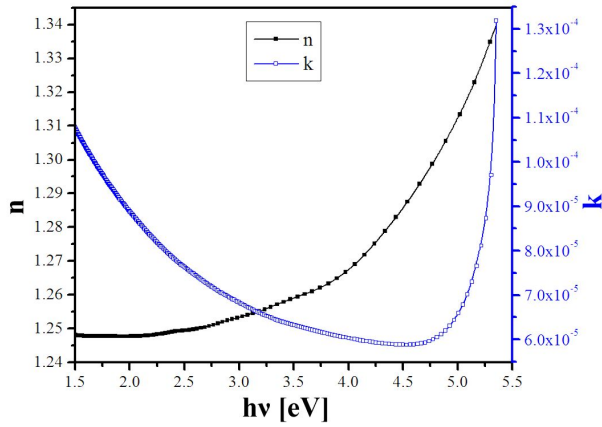


Fig. 4. The refractive index n and the extinction coefficient k of GHF single crystal.

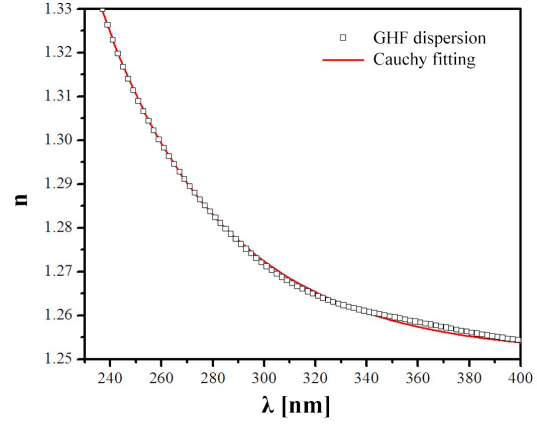


Fig. 5. Cauchy fitting of the refractive index n for GHF single crystal.

with good transparency in the visible region of the spectrum, thus, describes the normal dispersion of the refractive index which indicates that refractive index n monotonically decreases with increasing wavelength.

Fig. 5 presents the best fit of n with λ in nm (scattered dots represent the experimental refractive index) which yields the expression:

$$n(\lambda) = 1.258 - \frac{3234.685}{\lambda^2} + \frac{4.065 \times 10^8}{\lambda^4} \quad (6)$$

By extrapolating the refractive index values, expression 6 in the strong absorption region could be estimated as shown by the solid curve in Fig. 5. This indicates that GHF crystal belongs to the Cauchy dispersion type. The parameter A in equation 5 represents the static refractive index n_∞ which can be obtained at $\lambda \rightarrow \infty$.

Another way to explain the dispersion of refractive index has been developed by Wemple and DiDomenico (WDD) who suggested a model based on a single oscillator formula [14, 15]:

$$n^2 - 1 = \frac{E_d E_{so}}{E_{so}^2 - (h\nu)^2} \quad (7)$$

where E_d is the dispersion energy of a single oscillator and E_{so} is the single oscillator energy. The dispersion energy E_d represents the strength of the interband transition, while E_{so} represents the average excitation for electronic transitions.

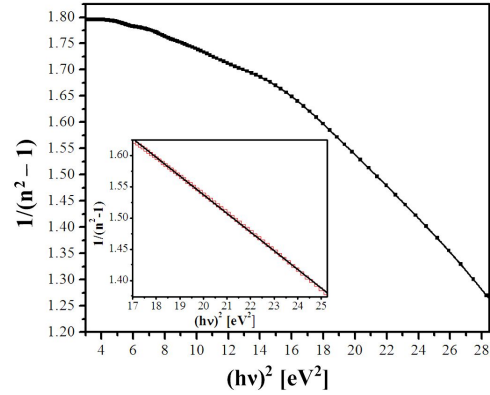


Fig. 6. Dispersion relation between $1/(n^2 - 1)$ and $(h\nu)^2$ for the GHF single crystal; the inset shows the area selected for the fitting.

WDD dispersion relation is plotted in Fig. 6, and values of E_d and E_{so} have been determined from the slope and the intercept of the linear portion of $\frac{1}{(n^2-1)}$ versus $(h\nu)^2$ plot and the calculated values are listed in Table 2. The obtained values differ from the corresponding values of glassy materials for many reasons, as the type of electronic transition in dielectric crystals is indirect interband transition which affects E_{so} value to be less than the calculated optical energy gap.

WDD model suggests a formula to calculate the oscillator wavelength as follows:

$$\frac{n_o^2 - 1}{(n^2 - 1)} = 1 - \left(\frac{\lambda_o}{\lambda}\right)^2 \quad (8)$$

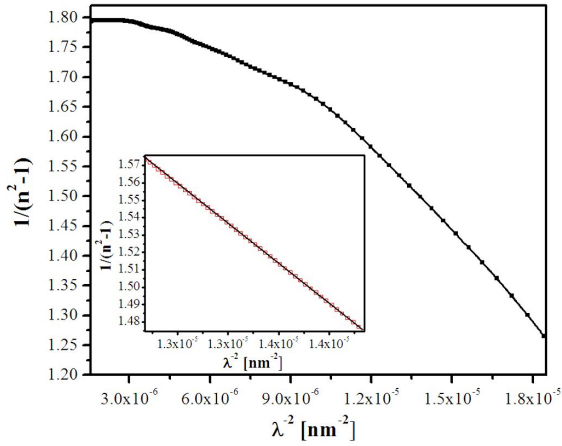


Fig. 7. $1/(n^2 - 1)$ versus λ^{-2} dispersion relation for GHF single crystal; the inset shows the area selected for the fitting.

where n_0 is a static refractive index which can be determined from equation 7 at diminishingly small energy value $h\nu \rightarrow 0$, λ_0 is known as oscillator wavelength. A graph between $(n^2 - 1)^{-1}$ versus $(\lambda)^{-2}$ is plotted in Fig. 7. The values of the static refractive index obtained from Cauchy and WDD models do not match perfectly as presented in Table 2. This deviation in the two models can be explained by the fact that WDD has been assigned to the linear portion at any spectrum range while the Cauchy model is applied only in the high absorption region.

To determine the value of the oscillator wavelength, a parameter SO_{st} can be introduced, by rearranging the oscillator equation:

$$\frac{1}{(n^2 - 1)} = \frac{1}{\lambda_0^2 SO_{st}} - \frac{1}{\lambda^2 SO_{st}} \quad (9)$$

where $SO_{st} = (n_0^2 - 1)/\lambda_0^2$ and the rearranged equation is known as single oscillator strength. Fig. 7 shows the dispersion of refractive index described by equation 9 and the inset shows the normal dispersion region selected for the fitting. There is a small deviation from linearity or a curvature in the refractive index at longer wavelengths or small energies as observed in Fig. 6 and Fig. 7. This deviation is due to negative contribution of lattice vibrations to the refractive index.

The GHF crystal dispersion behavior does not exhibit any anomalous dispersion in the measuring range which means that the incident radiation does not match with any absorption frequency of the crystal. A normal dispersion has been detected which is linear in the lower wavelength region. GHF crystal fits perfectly to the WDD model, thus, the crystal can be treated as a single oscillator with a wavelength in the UV region.

3.4.3. Lattice dielectric constant ϵ_L and contribution of charge carrier N/m^*

The data obtained for refractive index n can be analyzed to get the lattice dielectric constant ϵ_L . The relation between optical real part of dielectric constant ϵ_{real} and the square of wavelength λ^2 is given by [16]:

$$\epsilon_{real} = n^2 - k^2 = \epsilon_L - \frac{e^2}{4\pi^2 c^2 \epsilon_0} \frac{N}{m^*} \lambda^2 \quad (10)$$

where e is the electronic charge, ϵ_L is the dielectric constant, ϵ_0 is the permittivity of free space (8.854×10^{-12} F/m), c is the velocity of light, and N/m^* is the ratio of carrier concentration to the effective mass. The lattice dielectric constant and the carrier concentration ratio can be calculated from fitting of linear part representing the normal dispersion in the plot of n^2 versus λ^2 . The plot is presented in Fig. 8, and the obtained values of ϵ_L and N/m^* are listed in Table 2.

Table 2. Optical parameters for GHF crystal.

Parameter	Value
Dispersion energy E_{so} [eV]	8.453
Oscillator energy E_d [eV]	3.959
Static refractive index n_∞ from Cauchy formula	1.258
Static refractive index n_0 from WDD model	1.769
Oscillator wavelength λ_0 [nm]	146.29
Oscillator strength SO_{st} [nm^{-2}]	9.95×10^{-5}
lattice dielectric constant ϵ_L	1.872
The ratio of carrier concentration to the effective mass N/m^* [$\text{m}^3 \cdot \text{kg}^{-1}$]	3.52×10^{57}

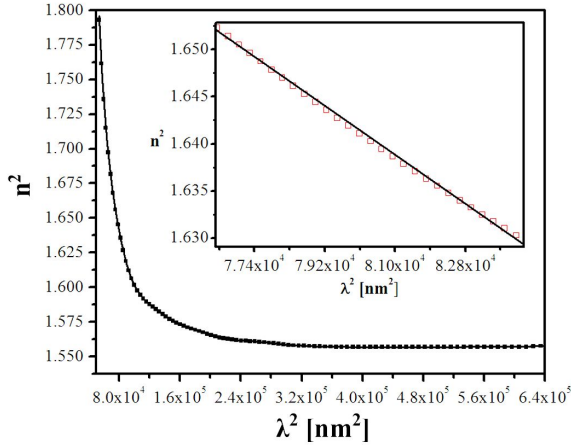


Fig. 8. The dispersion of n^2 versus λ^2 for GHF single crystal; the inset shows the area selected for fitting.

Another important optical parameter is a complex dielectric constant $\tilde{\epsilon}$ since the resonant modes or band structure of any material introduce spectral variation of dielectric constant. The importance of $\tilde{\epsilon}$ is that it may be associated with the design of optoelectronic devices [17]. The complex dielectric constant is described by the following relation:

$$\tilde{\epsilon} = \epsilon_{real} - i \epsilon_{im}. \quad (11)$$

The real ϵ_{real} and imaginary ϵ_{im} parts of the dielectric constant are related to n and k by the relations:

$$\epsilon_{real} = n^2 - k^2 \quad (12)$$

$$\epsilon_{im} = 2nk \quad (13)$$

The real part of the dielectric constant is associated with the speed of light attenuation within the material while the imaginary part explains how a dielectric absorbs energy from electric field [18].

Variations of the real and imaginary parts of the complex dielectric constant (ϵ_{real} , ϵ_{im}) with photon energy $h\nu$ for GHF crystal are displayed in Fig. 9, from which it is observed that the graph of real part of dielectric constant against energy is similar to that of refractive index. Also, there are no significant peaks in the spectra of the two parts of the dielectric constant

but the two curves intersect around incident photon energy of 3.1 eV. The two parts show an opposite behavior in the energy range of 2.2 eV to 4.5 eV which indicates an interaction between electrons and photons of the incident light in this range, after which the two curves exhibit significant increment resulting from polarization increase in the crystal at high energies or low wavelengths.

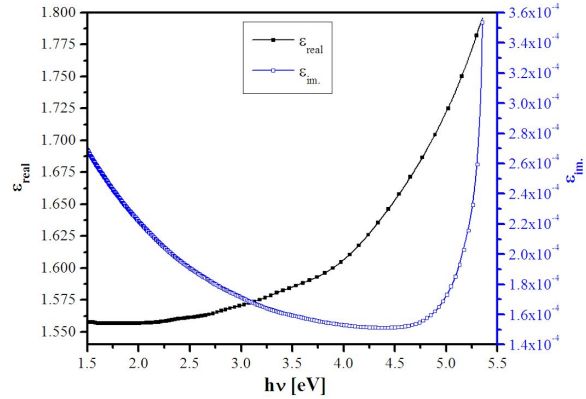


Fig. 9. Spectra of real ϵ_{real} and imaginary ϵ_{im} parts of the dielectric constant for GHF single crystal.

The real and imaginary parts of the dielectric constant can also be employed to calculate the spectral behavior of the real σ_1 and imaginary σ_2 optical conductivities according to the following relations [19]:

$$\sigma^* = \sigma_1 + i\sigma_2 \quad (14)$$

$$\sigma_1 = \omega \epsilon_o \epsilon_{im} \text{ and } \sigma_2 = \omega \epsilon_o \epsilon_{real} \quad (15)$$

where ω is the angular frequency, ϵ_o is the permittivity of free space. The spectral behavior of the real and imaginary optical conductivities in the photon energy range 1.5 eV to 5.4 eV is illustrated in Fig. 10.

The spectra in Fig. 10 show an opposite trend of the two parts of optical conductivity, as σ_1 increases slightly with increasing photon energy up to 4.9 eV after that it starts to increase rapidly with the increase of photon energy. The value of σ_2 decreases monotonically with increasing photon energy in the overall measuring range of photon energy.

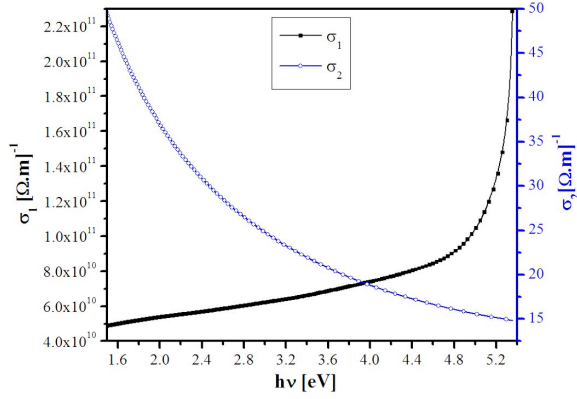


Fig. 10. Spectra of optical conductivities σ_1 and σ_2 for GHF single crystal.

3.5. Temperature dependence of optical band gap

The optical band gap of material can be determined from the UV-Vis transmittance spectra using Tauc expression [20] for allowed indirect optical transitions:

$$\omega^2 \alpha \propto (\hbar\omega - E_g)^2 \quad (16)$$

where α is the optical absorbance at photon energy $\hbar\omega$ and ω is the frequency of the incident radiation. An expression can be employed to determine the optical energy gap E_g by introducing the proportionality constant ν^2 :

$$\omega^2 \alpha = \nu^2 (\hbar\omega - E_g)^2 \quad (17)$$

The substitution of ω in terms of the wavelength λ in equation 17 and solving for α yields:

$$\frac{\sqrt{\alpha}}{\lambda} = \nu \frac{h}{2\pi\lambda} - \nu \frac{E_g}{2\pi c} \quad (18)$$

Thus, a plot of $\sqrt{\alpha}$ against λ should be a straight line. The fitting of the straight line yields a negative slope equal to $\nu \frac{E_g}{2\pi c}$ and an interception $\nu \frac{h}{2\pi}$ with the $\sqrt{\alpha}$ axis. In this way the optical energy gap E_g can be easily evaluated.

The spectral distribution of the optical absorption $\sqrt{\alpha}$ as a function of wavelength λ in the range of 200 nm to 800 nm was measured in the temperature range of 308 K to 358 K. From these results, the $\sqrt{\alpha} - \lambda$ dependence at different crystal

temperatures is exhibited in Fig. 11, which shows a typical Tauc plot with the inset showing the linear portion employed in the fitting. The general trend of α at any temperature shows a continuous decrease with increasing λ and the absorption edge is observed at low wavelengths where α increases more rapidly. The straight portion of the curve was then extrapolated and its intersection with the abscissa was determined. The band gap was then evaluated at different temperatures for GHF samples using equation 18.

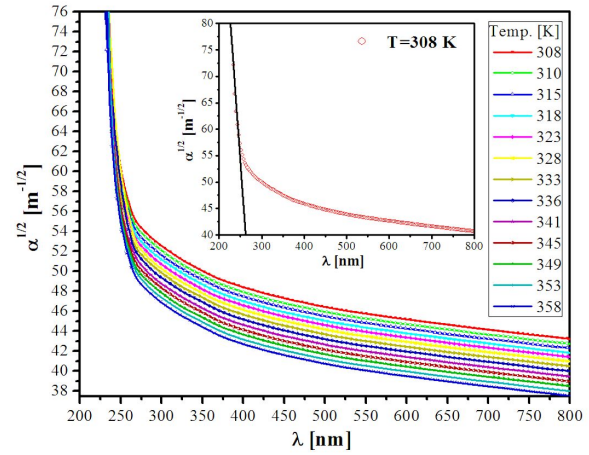


Fig. 11. Tauc plot for GHF single crystal at different crystal temperatures; the inset shows the fitting of the linear portion employed in calculating the optical energy gap.

The values of E_g vary linearly with temperature as depicted in Fig. 12. The calculated temperature gradient of the band gap $\partial E_g / \partial T$ is equal to -0.022 eV/K. Raising crystal temperature shifts the optical gap towards the lower energy side. The variation of the band gap energy may be attributed to the temperature dependent expansion or the lattice widening which induces a shift in relative positions of the valence and conduction bands with decrease in the optical transition energy. The relative positions of valence and conduction bands may also be shifted due to interactions between electrons and phonons.

The slight change in the band gap with increasing crystal temperature may also be due to irregular changes in the defect concentration present

in the structure in addition to the possibility of recombination processes as described in our previous work for $(\text{NH}_4)_2\text{ZnCl}_4[\text{K}_x(\text{NH}_4)_{1-x}]_2\text{ZnCl}_4$ and $(\text{TMA})_2\text{ZnCl}_4$ single crystals [21, 22]. Another hypothesis for the decrease of the indirect optical energy gap with increasing temperature has been proposed as thermal activation of the crystal resulting in increasing the phonon energy which can be associated with the indirect electronic transition. As a result, a total decrease in the energy of the indirect transition is observed [23].

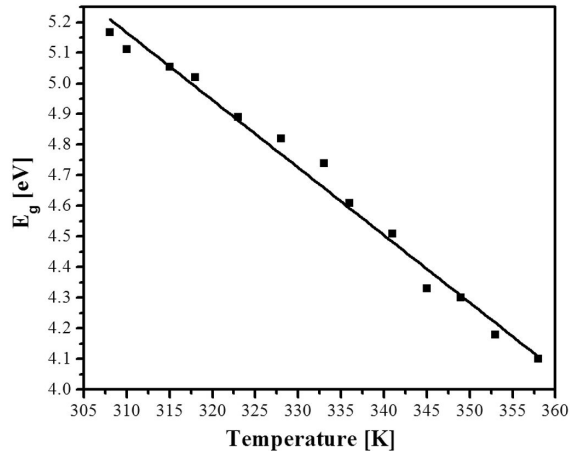


Fig. 12. Optical energy gap dependence on crystal temperature.

3.6. Urbach tail energy

The density of localized states could be estimated from Urbach rule [24]:

$$\alpha = \alpha_0 \exp(h\nu/E_e) \quad (19)$$

where α_0 is a constant and E_e is the Urbach tail energy which describes the width of the tails formed in the forbidden band gap due to the presence of localized states. To calculate the Urbach tail energy, a graph of $\ln\alpha$ versus $h\nu$ has been plotted (Fig. 13a) and from the straight portions of the curves the Urbach tail energy has been evaluated. The band tail energy E_e dependence on the temperature T is shown in Fig. 13b. The Urbach tail energy E_e shows a trend opposite to the optical energy gap E_g as it increases with increasing crystal temperature. This may be explained in terms of assumption that

the temperature increase results in an increase in unsaturated defects in the energy gap which increase the density of localized states of Urbach tail E_e in addition to a decrease in the optical energy gap values E_g .

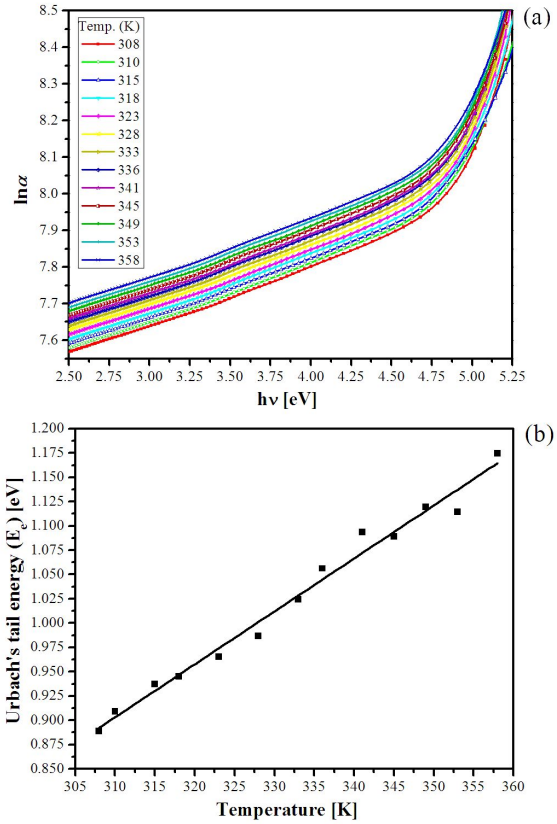


Fig. 13. (a) $\ln \alpha$ versus $h\nu$ at different temperatures for GHF single crystal; (b) Urbach tail energy dependence on the crystal temperature.

3.7. SHG investigation

The harmonic generation is a nonlinear optical process in which photons interacting with a nonlinear medium are effectively "combined" to form new photons. The nonlinearity in single crystal is observed under certain conditions such as interaction with an intense electromagnetic radiation. Second harmonic generation (SHG) is a nonlinear phenomenon observed when a crystal is irradiated with high intensity radiation. The incident photons induce polarization in the crystal caused

by the electric field of the electromagnetic radiation. This phenomenon cannot be observed in centrosymmetric structures. The technique employed in this investigation was developed by Kurtz et al. [25]. The employed powder technique is considered as an initial categorization of materials exhibiting SHG or not, and thus, screening materials for nonlinear optical applications.

In a typical measurement, Q-switched laser beam with a fundamental wavelength of 1064 nm was focused on a grinded powder of GHF single crystal in a nondestructive procedure. The energy delivered in each pulse, equal to 1.1 mJ per pulse with a repetition rate of 10 Hz and average of 256 shots, produced an output voltage confirming the harmonic generation or not. This output voltage was compared with the output voltages measured for potassium dihydrogen phosphate (KDP) and urea as reference samples as they showed the highest SHG efficiencies. GHF powder sample produced an output voltage equal to 17 mV, while the reference samples produced 72 mV and 28 mV for urea and KDP, respectively.

The calculated SHG efficiency of GHF sample is comparable to KDP as its output voltage equals to 0.607 output voltage of KDP at the operating conditions discussed previously. This result allows us to include the crystal into the SHG family and also provides the conclusion that GHF crystal does not possess a center of symmetry. Further modification of GHF crystal is possible by adding different dopants making it more efficient like in the case of doping KDP crystals with La^{+3} ions [26]. That point needs further investigations; therefore, we will take this study into consideration in the near future.

4. Conclusions

Glycine hydrofluoride (GHF) crystals were synthesized from aqueous solutions and a single crystal of good optical quality was obtained. The crystal in a powder form was subjected to X-ray investigation. The analysis revealed that GHF crystallizes in the orthorhombic crystal system with lattice parameters $a = 15.528 \text{ \AA}$, $b = 14.0949 \text{ \AA}$, $c = 15.749 \text{ \AA}$.

FT-IR spectra of GHF samples were measured between 4000 cm^{-1} and 400 cm^{-1} and the functional groups were identified and additional fluoride based bands were assigned.

Optical parameters, such as absorption coefficient α , extinction coefficient k , refractive index n , high frequency dielectric constant ϵ_L , optical conductivities σ_1 , σ_2 and the carrier concentration to the effective mass ratio N/m^* were determined. Single oscillator model was employed to analyze the normal dispersion of the refractive index. In addition, Cauchy model was applied to the refractive index in the high absorption region and the crystal demonstrated an excellent fitting to the formula. The absorption mechanism was found to be due to optical indirect transition, and the dependence of the absorption coefficient α on the incident photon wavelength λ in the spectral range of 200 nm to 800 nm was reported in the temperature range 308 K to 358 K. The indirect optical gap E_g was found to be strongly dependent on crystal temperature and showed a decreasing trend with increasing crystal temperature. Urbach tail energy E_c increased with increasing temperature showing an opposite behavior to the optical energy gap E_g . GHF single crystal has SHG efficiency of 0.607 compared with KDP crystal, and this result includes GHF into the SHG material family. It also proves that GHF does not crystallize in centrosymmetric structure.

Acknowledgements

The authors would like to thank Professor Puspendu K. Das and Professor C. Karthika (Department of Inorganic and Physical Chemistry, Indian Institute of Science Bangalore, India) for their effort and help in the second harmonic generation measurements.

References

- [1] FLECK M., PETROSYAN A.M., *Salts of Amino Acids: Crystallization, Structure and Properties*, Springer, Switzerland, 2014.
- [2] PAČESOVÁ S., BŘEZINA B., JASTRABÍK L., *Phys. Status Solidi B*, 2 (1983), 645.
- [3] MOSS T.S., BURRELL G.J., ELLIS E., *Semiconductor Optoelectronics*, Butterworths, London, 1973.
- [4] VIJAYAN N., BHAGAVANNARAYANA G., SHARMA S.N., DAS S., *J. Mater. Sci.*, 13 (2009), 3457.
- [5] SELVARAJU K., VALLUVAN R., KUMARARAMAN S., *Mater. Sci. Lett.*, 23 (2006), 2848.

- [6] FLECK M., GHAZARYAN V.V., PETROSYAN A.M., *J. Mol. Struct.*, 1 (2010), 83.
- [7] ROSADO M.T., DUARTE M.L.T., FAUSTO R., *Vib. Spectrosc.*, 1 (1998), 35.
- [8] IBRAHIM M., NADA A., KAMAL D.E., *Indian J. Pure Appl. Phys.*, 12 (2005), 911.
- [9] SOCRATES G., *Infrared and Raman characteristic group frequencies: tables and charts*, John Wiley & Sons, Chichester, 2001.
- [10] STUART B.H., *Infrared Spectroscopy: Fundamentals and Applications*, John Wiley & Sons, Chichester, 2004.
- [11] AL-FALEH R.S., ZIHLIF A.M., *Physica B*, 10 (2011), 1919.
- [12] ABU EL-FADL A., GAFFAR M.A., OMAR M.H., *Physica B*, 3 – 4 (1999), 403.
- [13] AL-KUHAILI M.F., *Opt. Mater.*, 3 (2004), 383.
- [14] WEMPLE S.H., DIDOMENICO M. JR., *Phys. Rev. B*, 4 (1971), 1338.
- [15] WEMPLE S.H., DIDOMENICO M. JR., *Phys. Rev. Lett.*, 20 (1969), 1156.
- [16] DAHSHAN A., AMER H.H., ALY K.A., *J. Phys. D: Appl. Phys.*, 21 (2008), 215401.
- [17] ZHOKHAVETS U., GOLDHAHN R., GOBSCH G., SCHLIEFKE W., *Synth. Met.*, 3 (2003), 491.
- [18] SHARMA P., SHARMA V., KATYAL S.C., *Chalcogenide Lett.*, 10 (2006), 73.
- [19] CAGLAR Y., ILICAN S., CAGLAR M., *Eur. Phys. J. B*, 3 (2007), 251.
- [20] TAUC J., GRIGOROVICI R., VANCU A., *Phys. Status Solidi B*, 2 (1996), 627.
- [21] GAFFAR M.A., ABU EL-FADL A., BIN ANOOZ S., *Cryst. Res. Technol.*, 9 (2003), 798.
- [22] ABU EL-FADL A., SOLTAN A.S., SHAALAN N.M., *Opt. Laser Technol.*, 7 (2007), 1310.
- [23] ABU EL-FADL A., NASHAAT A.M., *Open Mater. Sci. J.*, (2015), 162.
- [24] URBACH F., *Phys. Rev.*, 5 (1953), 1324.
- [25] KURTZ S.K., PERRY T.T., *J. Appl. Phys.*, 8 (1968), 3798.
- [26] KANNAN V., BAIRAVA GANESH R., SATHYALAKSHMI R., RAJESH N.P., RAMASAMY P., *Cryst. Res. Technol.*, 7 (2006), 678.

Received 2017-11-28

Accepted 2018-05-16